Journal of Magnetism and Magnetic Materials 433 (2017) 109–115

Contents lists available at ScienceDirect

Journal of Magnetism and Magnetic Materials

journal homepage: www.elsevier.com/locate/jmmm

Structure stability and magnetism in graphene impurity complexes with embedded V and Nb atoms

Jyoti Thakur [a], Manish K. Kashyap [b,c,*], Ankur Taya [b], Priti Rani [b], Hardev S. Saini [d], A.H. Reshak [e,f]

[a] Department of Physics, University College, Kurukshetra University, Kurukshetra 136119, Haryana, India
[b] Department of Physics, Kurukshetra University, Kurukshetra 136119, Haryana, India
[c] Ames Laboratory, U.S. Department of Energy, Iowa State University, Ames, IA 50011-3020, USA
[d] Department of Physics, Guru Jambheshwar University of Science & Technology, Hisar 125001, Haryana, India
[e] New Technologies – Research Centre, University of West Bohemia, Univerzitni 8, 306 14 Pilsen, Czech Republic
[f] School of Material Engineering, University Malaysia Perlis, 01007 Kangar, Perlis, Malaysia

ARTICLE INFO

Article history:
Received 2 January 2017
Received in revised form 21 February 2017
Accepted 3 March 2017
Available online 6 March 2017

Keywords:
DFT
FPLAPW
Spintronics
Graphene

ABSTRACT

The appearance of vacancy defects could produce appropriate magnetic moment in graphene and the sensitivity to absorb atoms/molecules also increases with this. In this direction, a DFT study of embedding V and Nb atom in graphene containing monovacancies (MV) and divacancies (DV) is reported. Complete/almost complete spin polarization is detected for V/Nb embedding. The origin of magnetism has been identified via interaction of *3d*-states of embedded atom with C-*p* states present in the vicinity of embedded site. The band structures have been analyzed to counter the observed semiconducting nature of graphene in minority spin on embedding V/Nb atom. The isosurface analysis also confirms the induced magnetism of present nanosystems. The present results reveal that these nanosystems have the potential for futuristic applications like spintronics and energy resources.

1. Introduction

A truly two-dimensional honeycomb structure of carbons atom is famous as "Graphene", which can be exfoliated from graphite in the form of one-atom thick monolayer [1]. Right from its discovery, graphene is considered as an excellent nanomaterial for possessing technological properties such as scalability, chemical stability, ballistic transport at room temperature [2,3], high mobility of charge carriers [4] and high elasticity [5]. Additionally, a weak spin-orbit interaction among carbon atoms leads to a long spin relaxation length on the surface of graphene [6]. Hence, graphene is a potential substitute for using in spintronic devices, recording media, magnetic inks, spin qubits, spin valves and nanomagnetic magnetism [7–10].

However, in spite of huge varieties of its novel applications, the use of graphene is rather limited due to its zero band gap [11,12]. Presently, many research efforts are directed towards inducing and fine tuning of the band gap in graphene [13,14]. Various approaches have been used to effectively induce and manipulate the magnetic states in graphene which are crucial for its use in nanoscale devices [15–17]. The production of magnetic carbon can be achieved via different routes like chemical vapor deposition [18,19], ion bombardment [20,21], nanofoam [22], ion implantation [23] etc. Spin polarized density functional theory (DFT) calculations of magnetic properties of the vacancies and vacancy-hydrogen complexes containing graphite [24] showed that these defects lead to a macroscopic magnetic signal as observed in experiments [20].

Experimental [25,26] and theoretical [27–29] investigations demonstrated that the most preferred way to incorporate transition metal (TM) impurities in graphene is to attach them to vacancies. Recently, Gan et al. [30] using high resolution transmission electron microscopy (HRTEM) observed substitutional Au and Pt atoms in graphene nanosheets increases the potential of graphene in spintronic applications. Wang et al. [31] found that a two-step process is an efficient way to dope graphene nanosheets; (i) first to create vacancies by high energy atom/ion bombardment and (ii) then to fill these vacancies with the desired dopant. Robertson et al. [32] were able to locally control the formation of mono- and di-vacancies in graphene at predefined sites with a focused electron beam at 80 keV, later these vacancies can also act as trap sites for mobile Fe atoms.

On the theoretical front, electronic and structural distortions in graphene induced by carbon vacancies and boron doping were

* Corresponding author at: Department of Physics, Kurukshetra University, Kurukshetra 136119, Haryana, India.
E-mail addresses: manishdft@gmail.com, mkumar@kuk.ac.in (M.K. Kashyap).

http://dx.doi.org/10.1016/j.jmmm.2017.03.005
0304-8853/

studied by Faccio et al. [33] and their results indicated that a boron atom behaves quite differently when occupies an atomic position near or far from vacancies. When it is far away/near from a vacancy, it slightly, enhances/destroys the magnetism in resultant nanosystem. Modelling of graphene containing monovacancies (MV), doped with O and B atoms was performed by Kaloni et al. [34] and their calculations demonstrated that B doping of oxidized vacancies is a successful approach to induce extended π-band magnetism. By controlling the O and B concentrations, it is possible to tune the magnetic state. Krasheninnikov et al. [35] explained the attractive interactions between transition metal atom impurities and vacancies in graphene using first-principles study. The electronic and magnetic properties of a graphene sheet decorated with TM atoms were investigated comprehensively using the first-principles calculations by Da et al. [36]. They found that TM-embedded graphene systems possess substantial magnetic moment with the maximum value of 3.5 μ_B in Mn-embedded graphene. Kang et al. [37] investigated the electronic structure and magnetic properties of substitutionally Mo-doped graphene from first-principles calculations and showed that this doping induces spin polarization and gives rise to a 2 μ_B spin magnetic moment on graphene. The various possible paths of oxygen reduction reaction (ORR) on MnN_4 embedded graphene (MnN_4-gra) were investigated by Lu et al. [38,39] using the dispersion-corrected density functional theory (DFT-D) method. They explored that the MnN_4-gra may have novel catalytic activity for ORR, at the cathode of hydrogen fuel cells. Lu et al. [40] also presented a systematic study on the geometry, adsorption energy and electronic structure of four different noble metal adatoms on graphdiyne (GDY).and found Rh and Ir adatoms on the GDY have the potential to be applied as single metal catalysts or gas molecule sensors.

The study of TM impurities in graphene simultaneously with the presence of vacancies is crucial step to examine the resultant electronic structure and to develop the physical understanding of bonding mechanism in metal-impurity graphene complexes. The physical properties of these complexes can be tuned by chemical and structural modification. Further, it is also essential to find out the origin of magnetism due to atomic defects in graphene nanomaterials. In present work, we plan to create the MV or divacancies (DV) in graphene nanosheets and filled one vacancy by a transition metal (X = V/Nb) dopants and examine the resultant nanostructure for spin polarization and magnetism. These two transition metals; V and Nb have been selected as both possess an equal number of d-electrons, respectively, thus the structural information and magnetic response of graphene impurity complexes can be determined by the size of V/Nb atom only. It is also aimed to realize how the TM gets strongly bound to defected graphene nanosheet and to observe the possible hybridization of C-sp^2 and TM-s,d orbitals. Further, an exhaustive comparison of peculiar electronic properties and magnetism of V- versus Nb- embedded graphene complex is also to be presented. This type of study is of prime importance as the resultant structures can be easily fabricated by electron irradiation to create defects first and depositing TM thereafter.

2. Computational details

The embedding of TM (X = V/Nb) impurity in graphene containing MV and DV were simulated by constructing $5 \times 5 \times 1$ supercell of graphene and a vacuum layer of 20 Å thick was inserted in the *z*-direction to avoid the interlayer interaction due to periodic boundary conditions. We employed density functional theory (DFT) [41] based projected augmented wave (PAW) method as implemented in VASP [42,43] for the relaxation of the systems under investigation. The generalized gradient approximation (GGA) as described by Perdew-Burke-Ernzerhof parameterization was used to construct exchange-correlation (XC) functional [44]. The PAW method is an all electron description and is used to describe the electron-ion description. The cut-off energy for plane waves was set to be 400 eV, a $9 \times 9 \times 1$ Monkhorst-Pack grid was used for sampling of the Brillouin zone during geometrical optimization. Conjugate gradient (CG) algorithm [45] was selected to relax present systems. All the internal coordinates were relaxed until calculated Hellmann Feymann force on each atom became less than 0.02 eV $Å^{-1}$. Several test calculations for higher supercells; $7 \times 7 \times 1$ and $8 \times 8 \times 1$ were also performed which gave essentially the same results.

After relaxation, we performed electronic structure calculations of relaxed systems using the full-potential linearized augmented plane-wave (FPLAPW) [46] method within GGA as implemented in WIEN2k package [47]. In FPLAPW calculations, the core states were treated fully relativistically, whereas for the valence states, a scalar relativistic approach was used. Additionally, valence electronic wavefunctions inside the Muffin-tin sphere were expanded up to $l_{max} = 10$. The radii of the Muffin-tin sphere (R_{MT}) for various atoms were taken such as to ensure almost touching spheres to avoid the possibility of charge leakage. The plane wave cut-off parameters were decided by $R_{MT}k_{max} = 7$ (where k_{max} is the largest wave vector of the basis set) and $G_{max} = 12$ a.u.$^{-1}$ for Fourier expansion of potential in the interstitial region. The k-space integration was carried out using modified tetrahedron method [48] with a k-mesh of $11 \times 11 \times 1$ for the high resolution and better convergence in the calculations.

3. Results and discussion

To begin with desired calculations, the graphene containing MV/DV was created by using $5 \times 5 \times 1$ supercell of pristine graphene and removing one/two adjacent C-atoms. Thereafter at one vacant site, foreign atom (X = V/Nb) was embedded and the structure so obtained was relaxed to find the actual atomic positions and possible bonding. It was found that on embedding V/Nb in graphene containing MV, the hexagonal symmetry near the vacant site remains maintained and the resultant nanosystem shows only substitutional effect with no shape transformation. However, embedding in graphene containing DV yields a shape change to the pentagonal structure at vacant sites via reordering of the chemical bonds between foreign V/Nb atom and C-atoms. The final relaxed structures in both cases are depicted in Fig.1. It is observed that embedded atom comes out of the graphene plane as the size of V/Nb atom is larger than C-atom.

In order to estimate the stability of a structure containing embedded TMs (X = V/Nb) atom in graphene nanosheets containing MV/DV, the binding energies (E_b^{MV+X}/E_b^{DV+X}) were calculated as under:

$$E_b^{MV+X} = E_{tot}^{MV+X} - (E_{tot}^{MV} + E_{tot}^{X}) \quad (1)$$

$$E_b^{DV+X} = E_{tot}^{DV+X} - (E_{tot}^{DV} + E_{tot}^{X}) \quad (2)$$

where $E_{tot}^{MV+X}/E_{tot}^{DV+X}$is the ground state energy of metal mono-/di-vacancy graphene complex and the bracketed terms in these equations represent the sum of ground state energies of reconstructed naked mono/di-vacancy; $E_{tot}^{MV}/E_{tot}^{DV}$ [20,49] and isolated TM (X) atom; E_{tot}. The computed binding energies are presented in Table 1. We observe that V-metal mono/di vacancy graphene complex is more energetically stable (Table 1) as compared to Nb-metal complex. Further, these findings are in good agreement with earlier reported works [37,50] i.e. binding energies of defected graphene are in ranges from −8 eV to −6 eV.

In case of embedding X-atom in graphene containing MV/DV, three/four neighbouring C-atoms constitute a bond with embed-

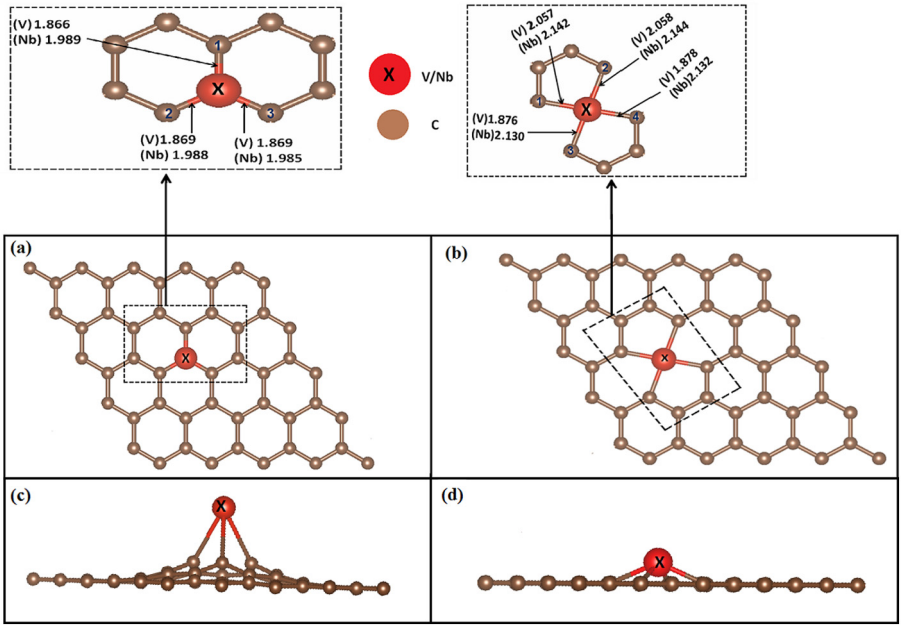

Fig. 1. Schematics for typical X = V/Nb atom embedding in graphene sheet containing (a) MV and (b) DV. Insets show the significant bond lengths of various C–X and C–C bonds in the vicinity of embedded site.

Table 1
Calculated bond lengths (Å) and binding energies (eV) of TM (X = V/Nb) atoms embedded in graphene sheet with (a) MV and (b) DV.

Embedded TM (X = V/Nb) in graphene containing MV/DV	E_b (eV)	Bond length (Å)	
MV	−7.892 (V)	V-C_1 = 1.866	Nb-C_1 = 1.989
	−6.584 (Nb)	V-C_2 = 1.869	Nb-C_2 = 1.988
		V-C_3 = 1.869	Nb-C_3 = 1.985
DV	−3.489 (V)	V-C_1 = 2.057	Nb-C_1 = 2.142
	−2.769 (Nb)	V-C_2 = 2.058	Nb-C_2 = 2.144
		V-C_3 = 1.876	Nb-C_3 = 1.878
		V-C_4 = 2.130	Nb-C_4 = 2.132

ded atom. There is a slight difference in relaxed bond lengths of various bonds (mentioned in Table 1) in all 4 cases but these are definitely larger than the standard C–C bond length (1.420 Å) of pristine graphene. Further, X-C bond length slightly increases for both MV and DV cases, as we move from embedding of V to Nb atom due to increase in the atomic size of latter.

Fig. 2 (upper panel) reveals the symmetrical DOS for pristine graphene in both spin channels which confirms its semimetallic nature [51]. On embedding the X atom (X = V/Nb) in MV/DV case (Fig. 2), the total DOS gets altered and localized levels start appearing, especially in the vicinity of Fermi level (E_F). The embedding of V/Nb atom in MV case generates complete spin polarization whereas, the same embedding in DV case yields large but not complete 100% spin polarization (Table 2). However, this much amount of polarization is also appreciable being capable of transporting spin polarized currents in spin quantum information devices and spin filter devices. The localized levels appearing in all embedded cases are the consequence of reformation of energy bands due to interaction of C-s and C-p states with d-states of foreign V/Nb atom.

To explore the contribution of various states in total DOS of resultant nanosystems, V-embedded graphene containing MV and DV were investigated (Fig. 3). It is found that V-d states and nearest neighbouring C-p states are located at E_F in majority spin channel whereas in minority spin, these states are almost absent.

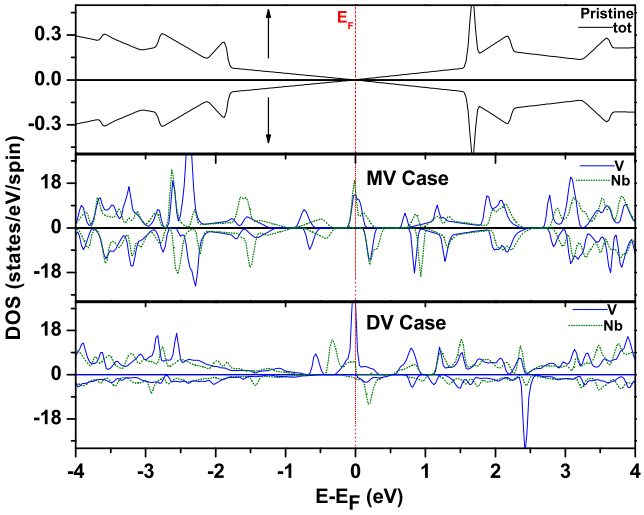

Fig. 2. Calculated spin polarized total density of states (TDOS) of pristine graphene, and V- and Nb-embedded graphene containing MV/DV.

This presents a direct evidence of interactions of V-d and C-p states on spin polarization. The C atoms away from embedded site (C_{far}) represent almost identical DOS in the vicinity of E_F, confirming that they play no role to decide any spin based conduction. In case of V-embedding in DV case, a small amount of minority DOS at E_F for V-d and C-p states is clearly visible that restrict maximum spin polarization in it. Nb-embedding in graphene containing MV/DV (not shown for brevity) can also be explained on the similar lines.

The bandstructure of V-doped graphene containing MV (Fig. 4) also confirms the half metallicity in minority spin channel as predicted by DOS plot. The present nanosystem contains direct bandgap along the K-K direction for this spin. Focusing on pristine graphene, it is well known that the energy bands depend only on the in-plane momentum of the electrons, whose movement is restricted by graphene's two-dimensional lattice, giving rise to

Table 2
Calculated spin polarization P(%), total spin magnetic moment M, spin moment on individual V/Nb atom ($M_{V/Nb}$), first/second nearest carbon atoms (M_{C1}/M_{C2}) and in interstitial region (M_{inter}) of X (X = V/Nb) embedded graphene containing MV/DV.

Graphene	P (%)	M(μ_B)	$M_{V/Nb}(\mu_B)$	$M_{C1}(\mu_B)$	$M_{C2}(\mu_B)$	$M_{inter}(\mu_B)$
MV	V = 100	1.35	0.689	0.028	0.027	0.121
	Nb = 100	0.99	0.737	0.035	0.034	0.033
DV	V = 98.6	3.35	1.866	0.118	0.116	0.832
	Nb = 95.6	2.30	1.095	0.114	0.112	0.228

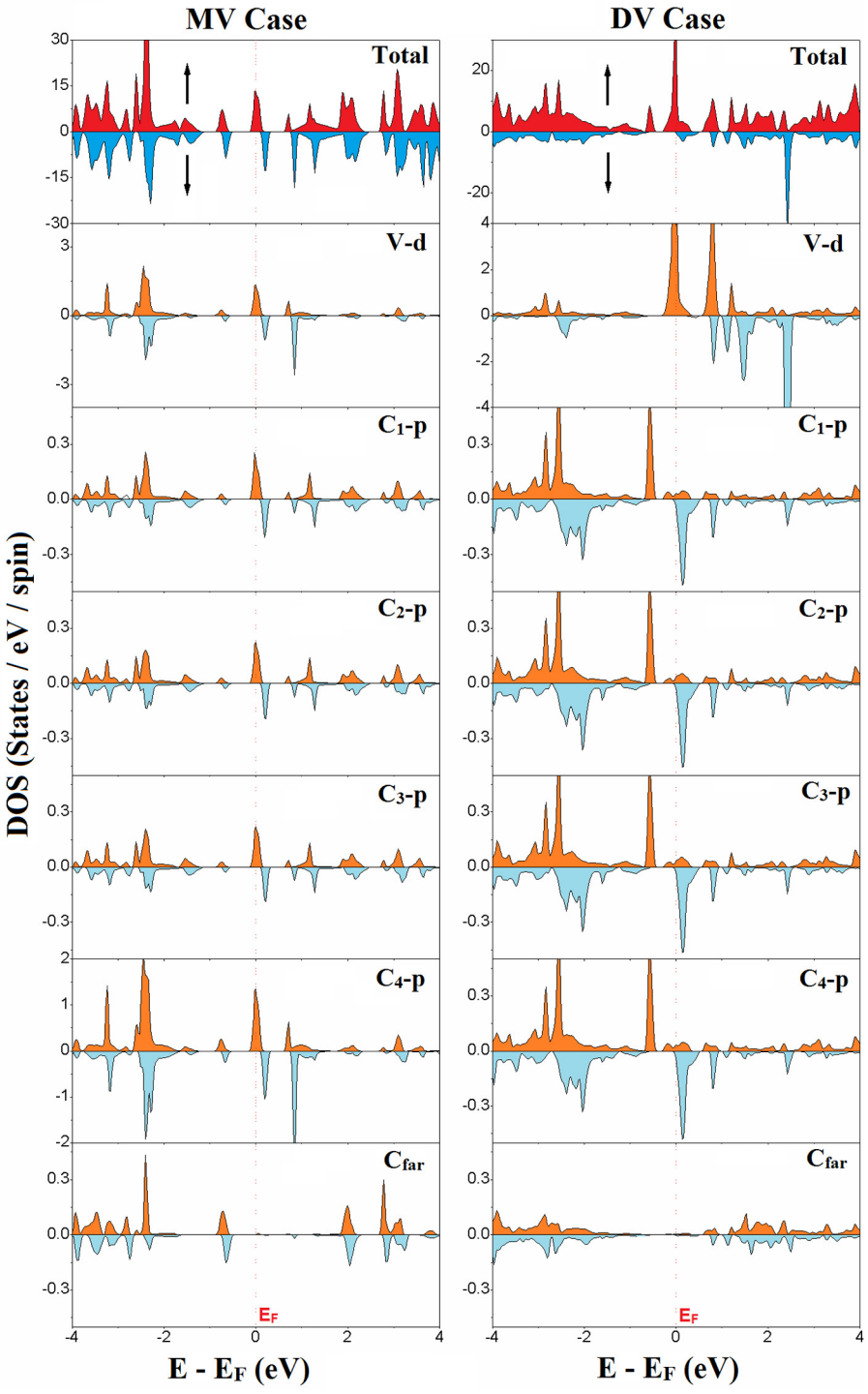

Fig. 3. Calculated spin resolved partial density of states (PDOS) of V-embedded graphene with MV/DV.

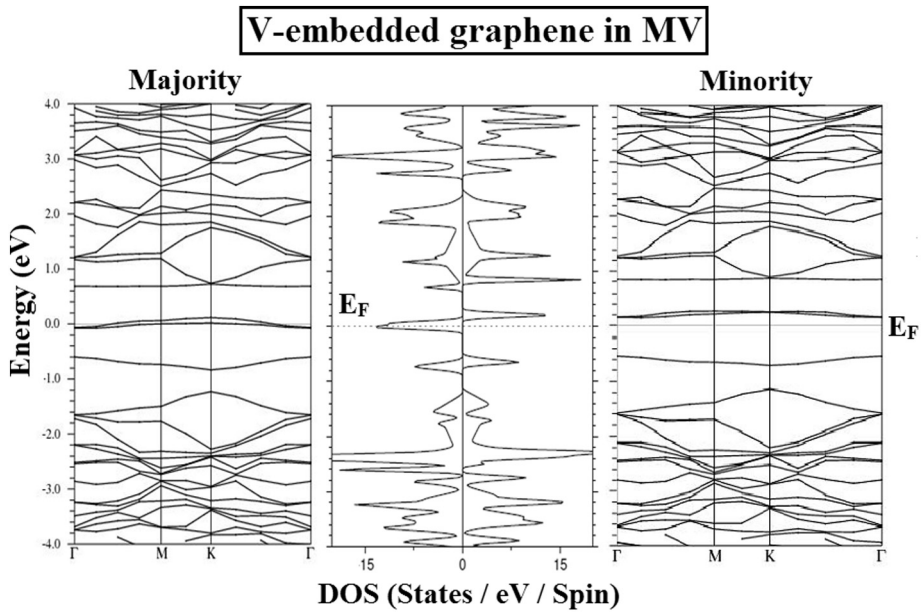

Fig. 4. Calculated spin polarized bandstructure along with total DOS of V-embedded graphene containing MV.

Dirac cone with zero gap. Two parts of Dirac cone, one each is valence and conduction band are the consequence of $\pi*$-antibonding and π bonding orbitals with vanishing carrier density at E_F, respectively. Now, the effect of adding V atoms in graphene containing MV is clearly visible. The alphabet 'V'-shaped valley is distorted and sublattice symmetry is broken. As a consequence, more and more **k**- points in the Brillion zone contribute to the DOS near E_F. This may be due to the transfer and redistribution of charges between graphene carbon atoms and dopant and thereby opening the π-$\pi*$ like bandgap in minority spin channel. This observation is in support of Zanolli's work [52] in which the band crossing and the splitting of spin-up/spin-down bands by doping of the graphene monolayer was verified. Further, large number of occupation states is still available in conduction band near E_F which can be easily populated via low energy excitation of electrons. Thus, the semiconducting properties can be drawn from minority spin channel of graphene which enhances its usefulness in nano optoelectronic devices. The perturbation in Dirac cone was also observed previously in F-, Ge-, Li- and K-intercalated graphene on SiC [53–55].

Pristine graphene has zero magnetic moment; but in X (X = V/Nb) embedded graphene nanosystems with MV/DV, C atoms in the vicinity of vacant site become non-equivalent. The X atom and non-equivalent C atoms containing spin polarized DOS induce the magnetic moment on graphene (Table 2). The total moment is proportional to net difference of DOS of electrons in two spin channels. Therefore, an appreciable moment of 1.33 μ_B/ 3.35 μ_B has been found in V embedded graphene containing MV/DV case. The corresponding moment in case of Nb embedding in MV/DV case is somewhat smaller than that in V-embedding. The other C atoms, which are away from embedded site, do not possess any significant magnetic moments. However, some moment is found to be distributed evenly in the interstitial regions among C atoms, which is also the case for g-B_3N_3C nanosheet; graphite like material [56]. Thus, this crucial moment should be considered for counting the total magnetic moment. V ($3d^3$ $4s^2$) atom has 5 valence electrons. Out of these, three valence electrons contribute to V-C σ covalent bonds in MV case. The fourth electron plays the same role as by that of missing C-atom at vacant site. This results in formation of equivalent π-bond, out of the plane of graphene. The additional electron left behind is free and can enter easily in non-bonding orbital. Due to this electron, the magnetic moment appears on graphene. The moment of Nb-embedded graphene containing MV is found lesser than that in V-embedded case due to presence of a radial node of Nb-4d orbital [27], resulting weaker p-d hybridization.

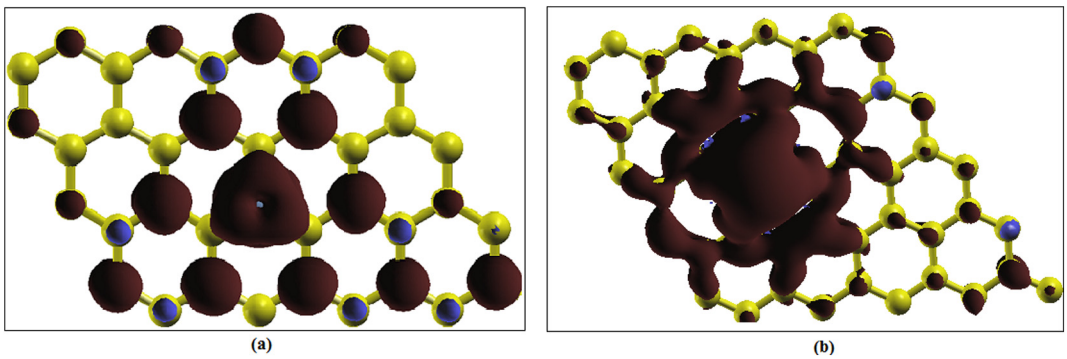

Fig. 5. Spin density difference isosurfaces for X (X = V/Nb) embedded graphene for (a) MV and (b) DV cases. The isosurfaces correspond to a value of 3×10^{-3} electrons/Å^3. Brown/blue color represents positive/negative values of accumulated spin density.

Other the other hand, the magnetic behaviour of these complexes in DV is found to be more interesting. It is observed that V/Nb embedding in graphene containing DV results in a "cross" configuration (Fig. 1). A larger "hole" at the di-vacancy site produces weaker interaction of the embedded atom with the ligand bonds which yields higher spin state of the complex. On applying similar logic to V-embedding in DV case, we found that the foreign V atom makes four local σ bonds with nearby C atoms (Fig. 1). Still one extra electron remains unsaturated on V-atom. Further, the V-C bond length is large in this case which enhances localization of the additional electron on V-atom. The formation of σ bonds and more localization increases the availability of the more states for free electrons due to which the magnetic moment enhances up to 3.35 μ_B. A similar reason may be quoted for the decrease in magnetic moment for Nb embedded graphene containing DV as in MV case (Table 2).

Finally, the isosurface analysis is also performed to confirm the magnetic ordering in the present nanosystems. To analyse the same, we have represented spin density difference isosurfaces $\Delta\rho(r)$ for V embedding in graphene for (a) MV and (b) DV in Fig. 5, where

$$\Delta\rho(r) = \rho_{MAC}(r) - \rho_{MIC}(r) \quad (3)$$

The positive value of $\Delta\rho(r)$ indicates the existence of magnetic moment in a specific region near the vacancy in both MV and DV cases. This results in stable ferromagnetic state for both cases. Further, $\Delta\rho(r)$ is more positive in DV case as due to presence of more unsaturated dangling bonds, thus, the availability of free electrons in the vicinity of E_F increases. This governs the enlarged moment for DV case. Qualitatively, our findings agree well with previous reports for 3d transition metal atoms decorated graphene [57–60].

4. Conclusions

The electronic and magnetic properties of X embedded (X = V and Nb) graphene with MV/DV have been studied using density functional theory (DFT) approach. Our calculations suggested that the electronic properties and magnetic response of graphene containing MV/DV get modified drastically on embedding V or Nb atom. The bandstructures of present nanosystems were analysed to identify the shifting of Dirac cone of graphene and hence to justify the semiconducting behaviour of graphene in minority spin channel. The isosurfaces plots confirmed the stability of ferromagnetic state of graphene on embedding V/Nb atoms. The magnetic moment is mainly contributed by doped TM atom with appreciable contributions from nearby C atoms as well. Complete/almost complete spin polarization is obtained for V and Nb embedded graphene containing MV/DV which makes resultant nanosystems appropriate materials for the development of spintronic devices, spin filter and injector devices. Since the presence of transition metal impurities could be detected easily by scanning tunnelling microscopy (STM), high resolution transmission electron microscopy (HRTEM) and X-ray absorption technique, thus the present investigations leave a definite experimental scope to work with the nanosystems under investigation.

Acknowledgement

The computation in this work was performed using the facility available at Department of Physics, Kurukshetra University, Kurukshetra (Haryana), India. For the author – A. H. Reshak, the result was developed within the CENTEM project, reg. no. CZ.1.05/2.1.00/03.0088, cofunded by the ERDF as part of the Ministry of Education, Youth and Sports OP RDI programme and, in the follow-up sustainability stage, supported through CENTEM PLUS (LO1402) by financial means from the Ministry of Education, Youth and Sports under the "National Sustainability Programme I. Computational resources were provided by MetaCentrum (LM2010005) and CERIT-SC (CZ.1.05/3.2.00/08.0144) infrastructures". We acknowledge the help and support from Dr. T. P. Kaloni, California State University, Northridge, United States for discussion of some crucial points in this manuscript.

References

[1] K.S. Novoselov, A.K. Geim, S.V. Morozov, D. Jiang, Y. Zhang, S.V. Dubonos, I.V. Grigorieva, A.A. Firsov, Science 306 (2004) 666.
[2] K.S. Novoselov, Z. Jiang, Y. Zhang, S.V. Morozov, H.L. Stromer, U. Zeitler, J.C. Maan, G.S. Boebinger, P. Kim, A.K. Geim, Science 315 (2007) 1379.
[3] K.I. Bolotin, K.J. Sikes, Z. Jiang, M. Klima, G. Fudenberg, J. Hone, P. Kim, H.L. Stormer, Solid State Commun. 146 (2008) 351.
[4] A.K. Geim, K.S. Novoselov, Nature Mater. 6 (2007) 183.
[5] L.E. Hueso, J.M. Pruneda, V. Ferrai, G. Burnell, J.P.V. Herrera, B.D. Simons, P.B. Littlewood, A. Fert, A. Emilio, N.D. Mathur, Nature 445 (2007) 410.
[6] T. Ohta, A. Bostwick, T. Seyller, K. Horn, E. Rotenberg, Science 313 (2006) 951.
[7] J. Thakur, M.K. Kashyap, H.S. Saini, A.H. Reshak, J. Alloys Compds. 649 (2015) 1300.
[8] J. Thakur, M.K. Kashyap, H.S. Saini, A.H. Reshak, J. Alloys Compds. 663 (2016) 100.
[9] J. Thakur, M.K. Kashyap, A. Taya, P. Rani, H.S. Saini, Indian J. Phys. 91 (2017) 43.
[10] M.K. Kashyap, T. Nautiyal, S. Auluck, J. Alloys Compds. 486 (2009) 60.
[11] A.H.N. Castro, F. Guinea, N.M.R. Peres, K.S. Novoselov, A.K. Geim, Rev. Mod. Phys. 81 (2009) 109.
[12] K.S. Novoselov, S.V. Morozov, T.M.G. Mohinddin, L.A. Ponomarenko, D.C. Elias, R. Yang, I.I. Barbolina, P. Blake, T.J. Booth, D. Jiang, J. Giesbers, E.W. Hill, A.K. Geim, Phys. Status Solidi B 244 (2007) 4106.
[13] S. Mukherjee, T.P. Kaloni, J. Nanopart. Res. 14 (2012) 1059.
[14] T.P. Kaloni, N. Singh, U. Schwingenschlögl, Phys. Rev. B 89 (2014) 035409.
[15] Y.S. Dedkov, M. Fonin, New J. Phys. 12 (2010) 125004.
[16] C. Cao, M. Wu, J.Z. Jiang, H.P. Cheng, Phys. Rev. B 81 (2010) 205424.
[17] Y. Mao, J. Yuan, J. Zhong, J. Phys.: Condens. Matter. 20 (2008) 115209.
[18] A.W. Mombru, H. Pardo, R. Faccio, O.F. de Lima, E.R. Leite, G. Zanelatto, A.J.C. Lanfredi, C. Cardoso, F.M. Araujo-Moreira, Phys. Rev. B 71 (2005) 100404.
[19] H. Pardo, R. Faccio, A.W. Mombru, F.M. Araujo-Moreira, O.F. Delima, Carbon 44 (2006) 565.
[20] P. Esquinazi, D. Spemann, R. Hohne, A. Setzer, K.H. Han, T. Butz, Phys. Rev. Lett. 91 (2003) 227201.
[21] P. Esquinazi, A. Setzer, R. Hohne, C. Semmelhack, Y. Kopelevich, D. Spemann, T. Butz, B. Kohlstrunk, M. Losche, Phys. Rev. B 66 (2002) 024429.
[22] A.V. Rode, E.G. Gamaly, A.G. Christy, J.G. Fitz Gerald, S.T. Thyde, R.G. Elliman, B. Luther-Davies, A.I. Veinger, J. Androulakis, J. Giapintzakis, Phys. Rev. B 70 (2004) 054407.
[23] T. Makarova, F. Palacio, Carbon-Based magnetism: An Overview of Metal Free Carbon-based Compounds and Materials, Elsevier, Amsterdam, 2005.
[24] Y. Ma, P.O. Lehtinen, A.S. Foster, R.M. Nieminen, Phys. Rev. B 72 (2005) 085451.
[25] O. Cretu, A.V. Krasheninnikov, J.A. Rodriguez-Manzo, L. Sun, R. Nieminen, F. Banhart, Phys. Rev. Lett. 105 (2010) 196102.
[26] M.M. Ugeda, I. Brihuega, F. Guinea, J.M. Gómez-Rodríguez, Phys. Rev. Lett. 104 (2010) 096804.
[27] J. Thakur, H.S. Saini, M. Singh, A.H. Reshak, M.K. Kashyap, Physica E 78 (2016) 35.
[28] E.J.G. Santos, A. Ayuela, S.B. Fagan, J. Mendes Filho, D.L. Azevedo, A.G. Souza Filho, D. Sanchez-Portal, Phys. Rev. B 78 (2008) 195420.
[29] E.J.G. Santos, A. Ayuela, D. Sanchez-Portal, New J. Phys. 12 (2010) 053012.
[30] Y. Gan, L. Sun, F. Banhart, Small 4 (2008) 587.
[31] H. Wang, Q. Wang, Y. Cheng, K. Li, Y. Yao, Q. Zhang, C. Dong, P. Wang, U. Schwingenschlögl, W. Yang, X.X. Zhang, Nano Lett. 12 (2012) 141.
[32] A.W. Robertson, B. Montanari, K. He, J. Kim, C.S. Allen, Y.A. Wu, J.H. Warner, Nano lett. 13 (2013) 1468.
[33] R. Faccio, L. Fernández-Werner, H. Pardoa, C. Goyenola, O.N. Venturab, Á.W. Mombrúa, J. Phys. Chem. C 114 (2010) 18961.
[34] T.P. Kaloni, M.U. Kahaly, R. Faccio, U. Schwingenschlögl, Carbon 64 (2013) 281.
[35] A.V. Krasheninnikov, R.M. Nieminen, Theo. Chem. Acc. 129 (2011) 625.
[36] H. Da, Y.P. Feng, G. Liang, J. Phys. Chem. C 115 (2011) 22701.
[37] J. Kang, H. X. Deng. S. S. Li, J. Li, J. Phys.: Conden. Matter 23 (2011) 346001.
[38] Z. Lu, G. Xu, C. He, T. Wang, L. Yang, Z. Yang, D. Ma, Carbon 84 (2015) 500.
[39] X. Zhang, Z. Lu, Y. Tang, Z. Fu, D. Ma, Z. Yang, Phys. Chem. Chem. Phys. 16 (2014) 20561.
[40] Z. Lu, S. Li, P. Lv, C. He, D. Ma, Z. Yang, Appl. Surf. Sci. 360 (2016) 1.
[41] M. Weinert, E. Wimmer, A.J. Freeman, Phys. Rev. B 26 (1982) 4571.
[42] G. Kresse, J. Furthmüller, Comp. Mater. Sci. 6 (1996) 15.
[43] G. Kresse, J. Furthmüller, Phys. Rev. B 54 (1996) 11169.
[44] J.P. Perdew, K. Burke, M. Ernzehof, Phys. Rev. Lett. 77 (1996) 3865.
[45] R.P. Feynman, Phys. Rev. 56 (1939) 340.
[46] G.K.H. Madsen, P. Blaha, K. Schwarz, E. Sjöstedt, L. Nordström, Phys. Rev. B 64 (2001) 195134.
[47] P. Blaha, K. Schwarz, G. Madsen, D.K. J. Luitz, Wien2k, An Augmented Plane Wave plus Local orbitals program for calculating crystal properties, Vienna University of technology, Austria, 2001, ISBN: 3-9501031-1-2.

[48] P.E. Blöchl, O. Jepsen, O.K. Andersen, Phys. Rev B 49 (1994) 16223.
[49] A.A. El-Barbary, R.H. Telling, C.P. Ewels, M.I. Heggie, P.R. Briddon, Phys. Rev. B 68 (2003) 144107.
[50] A.V. Krashenninnikov, P.O. Lehtinen, A.S. Foster, Phys. Rev. Lett. 102 (2009) 126807.
[51] A.W. Robertson, B. Montanari, K. He, C.S. Allen, Y.A. Wu, N.M. Harrison, J. H. Warner ACS Nano 7 (2013) 4495.
[52] Z. Zanolli, Scientific Reports 6 (2016) 31346.
[53] Y.C. Cheng, T.P. Kaloni, G.S. Huang, U. Schwingenschlögl, Appl. Phys. Lett. 99 (2011) 053117.
[54] T.P. Kaloni, Y.C. Cheng, M. UpadhyayKahaly, U. Schwingenschlögl, Chem. Phys. Lett. 534 (2012) 29.
[55] T.P. Kaloni, M. UpadhyayKahaly, Y.C. Cheng, U. Schwingenschlögl, Euro, Phys. Lett. 98 (2012) 67003.
[56] J. Li, D. Gao, X. Niu, M. Si, D. Xue, Nano. Res. Lett. 7 (2012) 624.
[57] M. Wu, C. Cao, J.Z. Ziang, New J. Phys. 12 (2012) 063020.
[58] T.P. Kaloni, N. Singh, U. Schwingenschlögl, Phys. Rev. B 89 (2012) 035409.
[59] T.P. Kaloni, S. Gangopadhyay, N. Singh, B. Jones, U. Schwingenschlögl, Phys. Rev. B 88 (2013) 235418.
[60] T.P. Kaloni, J. Phys. Chem. C 118 (2014) 25200.